Carbon 144 (2019) 628–638

Contents lists available at ScienceDirect

Carbon

journal homepage: www.elsevier.com/locate/carbon

Carbon nanotube/carbon composite fiber with improved strength and electrical conductivity via interface engineering

Songlin Zhang, Ayou Hao, Nam Nguyen, Abiodun Oluwalowo, Zhe Liu, Yourri Dessureault, Jin Gyu Park*, Richard Liang

High-Performance Materials Institute, Department of Industrial and Manufacturing Engineering, FAMU-FSU College of Engineering, Florida State University, 2005 Levy Ave., Tallahassee, FL, 32310, USA

ARTICLE INFO

Article history:
Received 15 November 2018
Received in revised form
18 December 2018
Accepted 23 December 2018
Available online 24 December 2018

Keywords:
Carbon/carbon composite
Carbon nanotube/carbon matrix composite
Pyrolyzed polydopamine (py-PDA)
Composite interface engineering
Electrical conductivity

ABSTRACT

Carbon nanotube/carbon (CNT/C) composites show potential for lightweight structural materials and non-metal electrical conductors for aerospace, military, and other industries where the combination of lightweight, high strength and excellent conductivity are required. Most research attempts have been reported to fabricate CNT/C composite focusing on the high CNT alignment and dense carbon matrix. However, simultaneous improvement of strength and electrical conductivity in materials still presents a great challenge. In this study, pyrolyzed polydopamine (*py*-PDA) with selected surface treatments is introduced as an interface enhancer between CNTs and the carbon matrix. Due to the presence of *py*-PDA, the effective physical interlocking and conductive pathways are rebuilt at the interface area between CNTs and carbon matrix, resulting in better load transfer and electron transport. The CNT/*py*-PDA/C composite fibers demonstrated remarkable improvements in electrical conductivity (2.1×10^3 S cm^{-1} or 228 S m^2 kg^{-1}) and tensile strength (up to 727 MPa or 790 MPa/(g·cm^{-3})), which should prove to be vastly advantageous as compared to the previously reported CNT/C composites. The outstanding thermal stability of fully carbonized materials is also an attractive feature. Coupled with scalable manufacturing methods, these integrated characteristics of CNT/*py*-PDA/C composite fiber can potentially have broad applications for lightweight structural materials and non-metal conductors.

1. Introduction

To advance technologies and developments in the aerospace and automotive fields, the next-generation of lightweight structural materials must be mechanically strong and electrically conductive with other multi-functionalities to meet the needs of future vehicle and aircraft applications [1–4]. As of now, carbon fiber (CF) has been extensively studied and possesses high specific tensile strength and modulus, as well as moderate conductivity [5], which originates from the highly ordered hexagonal carbon structure with low defect density [6]. Recently, researchers devoted great efforts in exploring other carbon allotropes, such as carbon nanotubes (CNTs), which show a much higher tensile strength of up to 100 GPa and modulus of up to 1.3 TPa [7,8] with a typical diameter of sub-nanometer to tens of nanometer [7]. Coupled with the exceptionally high electrical and thermal conductivities [9–11], CNTs could prove to be the answer for the next-generation of strong, light, and multifunctional reinforcement materials.

To meet additional requirements, including low thermal expansion coefficient, fire retardancy, and high working temperature of the aerospace industry, carbon or ceramic matrix composites have shown promise. When paired with nanomaterial reinforcements, the composite may realize the full advantages of the excellent properties of reinforcements including CNTs and graphene [2,12–19]. For instance, CF/carbon composites attract a lot of interest because of their high mechanical properties at elevated temperature in inert gas [2]. To date, carbon nanotube/carbon (CNT/C) composites have been reported with main focus on mechanical properties [13–15,20] and the structural evolution mechanism of carbon matrix [15,21,22]. Electrical properties have garnered less interest due to the poor conductive performance [23].

The carbon matrix of CNT/C composites are typically prepared through two routes: chemical vapor infiltration (CVI) [14,15,20–22,24] and polymer-infiltration-pyrolysis (PIP) [13,23]. Both methods strive to achieve strong and conductive CNT/C

* Corresponding author.
E-mail address: jgpark@fsu.edu (J.G. Park).

https://doi.org/10.1016/j.carbon.2018.12.091
0008-6223/

composites by increasing the alignment degree of the reinforcing CNTs [23], densifying the CNT network [14], and/or creating a highly graphitized carbon matrix in the vicinity of CNTs [21,25]. For instance, a multiple mechanical stretching process was applied to a CNT film by Han et al. [23] to prepare an aligned CNT/phenolic preform for C/C composite manufacturing using the PIP method. Jin et al. [14] used a pressed multi-wall carbon nanotube (MWCNT) block as a compact network for the subsequent carbon matrix deposition via the CVI route. In our previous work, CNT/C composites with a high CNT volume fraction was obtained by multiple carbon precursor infiltration using PIP method to achieve a fully densified carbon matrix [25]. The reported tensile strength of CNT/C composites ranged from 148.6 MPa to 460 MPa [13,14,26] as different parameters were optimized. A higher value of 1.7 GPa was also reported [15,20]. However, the electrical conductivity was either rarely evaluated or very low, ranging from 100 to 500 S cm^{-1} [13,14,25,26]. Although the better electrical performance of CNT/C composites has been achieved using the CVI method, results were still less than 1000 S cm^{-1} [23,27]. Furthermore, little attention was given to the effects of the interface between CNTs and carbon matrix on the mechanical and electrical performance of CNT/C composites.

The strategies of cross-linking and covalent bonding of CNT/polymer composites through reactions of oxygen (O) or nitrogen (N) containing functional groups [28,29] have not proven effective for improving the mechanical properties of CNT/C composite due to the decomposition of O/N functional groups after thermal treatment at high temperature [30–32]. Thus, weak interface interactions are expected between CNT and carbon matrix. Nevertheless, the carbon matrix enhances the inter-connections between CNTs by filling the pores within CNT networks [25,33], which can facilitate the load transfer among neighboring CNTs. Therefore, an effective interface design should be of great interest to simultaneously improve the mechanical and electrical properties of CNT/C composites [34,35]. However, only few results on the interface design of C/C composites are discussed in literature [32].

Polydopamine (PDA), an organic adhesive protein, has been a widely investigated multifunctional polymer because of its amazing characteristics, including extraordinary adhesion on various substrates [36–39]. After carbonization at high temperature, the strong adhesive properties of pyrolyzed polydopamine (*py*-PDA) are maintained [36]. This adhesive effect of *py*-PDA is important and different from the aforementioned cross-linking or covalent bonding via O/N containing functional groups [37]. Another advantage of *py*-PDA is that it is a highly electrical and thermal conductive carbon material [36,37]. Previous studies showed that *py*-PDA could be highly conductive, up to 10^3 S cm^{-1} [40–42]. Recently, a rough, hierarchical coating surface of *py*-PDA on reduced graphene oxide nanosheets was found to effectively improve the tensile properties of graphene fiber because of an enhanced physical interlock effect [36]. These characteristics of *py*-PDA can be possibly utilized as interface enhancer to prepare mechanically strong and electrically conductive CNT/C composites. However, to date, the interface engineering using *py*-PDA as an interface enhancer has not been explored to fabricate both strong and conductive CNT/C composite.

Herein, this study involved preparing *py*-PDA functionalized CNT/C composite fiber (referred to as CNT/*py*-PDA/C) by first coating PDA onto the CNTs, followed by carbon precursor infiltration, mechanical twisting, curing, and thermal treatment. The pyrolyzing process converted the interfaced PDA into conductive carbons of *py*-PDA. As-prepared, CNT/*py*-PDA/C fibers demonstrated greater tensile strength and higher electrical conductivity. Through tuning the concentration of carbon precursor solution and careful interface design of *py*-PDA, the CNT/*py*-PDA/C composite fibers were found to have tensile strength and modulus of up to 727 MPa and 85 GPa, respectively. More importantly, the electrical conductivity reached up to 2.1×10^3 S cm^{-1}, which, to the best of our knowledge, is the highest value reported for CNT/C composite fiber. Additionally, our fabrication method is readily modifiable for large-scale manufacturing and could assist with research of CNT/C composites including film (2D) or block/foam (3D) structures with a better understanding on the interface engineering. Together with these key finding, significant improvements of both mechanical and electrical properties of the resultant CNT/*py*-PDA/C composite fiber indicates the key potential role of the interface for CNT/C composite manufacturing.

2. Experimental section

2.1. CNT/py-PDA/C composite fiber manufacturing

CNT ribbon (CNTR) from Nanocomp Technologies Inc. was used as received without any pre-treatment. Floating catalyst chemical vapor deposition method was applied to grow CNTs yielding a continuously collected roll of CNTR. It is porous and usually contains amorphous carbon and iron metal catalyst. First, the raw CNTR (Fig. 1a1) was dipped into a dopamine solution (2 mg ml^{-1} in 10 mM tri-HCl buffer, pH of 8.5, Sigma-Aldrich Inc.) for 5, 10, 30, 60, and 120 min. Polydopamine (PDA) formed on the surface of CNTs through an auto-oxidative reaction (referred to as CNTR/PDA, step I in Fig. 1a2) [36,43]. Then phenolic resin (Durite™ Resin SC-1008, Hexion Inc.) in acetone with a concentration of 3, 5, and 10 wt.% was infiltrated into the CNTR/PDA for 2 h. The CNTR/PDA was further manually twisted into CNT fibers (referred to as CNT/PDA/Resin fiber). For clarification, samples were named as CNTR/XX before manual twisting, and CNT/YY fiber after manual twisting due to the shape difference where XX or YY represents various treatments such as PDA coating or resin infiltration. A curing process at 170 °C for 3 h, based on DSC results (Fig. S1a, Supporting Information), was carried out to facilitate phenolic resin molecules cross-linking (step II in Fig. 1a3).

Thermal treatment of fibers at various temperatures (800, 1000, and 1200 °C) was carried out in argon atmosphere using a tube furnace (GSL-1600X-OTF, MTI Corporation) to convert phenolic resin into a carbon matrix and PDA to *py*-PDA. The prepared fiber was referred to as CNT/*py*-PDA/C fiber (step III in Fig. 1a4). The initial carbonization was started at room temperature, increasing to 400 °C at 10 °C min^{-1} then held for 1 h. With a step-carbonization of every 100 °C at 5 °C·min^{-1}, it was held for 1 h at each temperature of 500, 600, 700, and 800 °C (Fig. S2, Supporting Information). For the cases of carbonization at 1000 and 1200 °C, the temperature was raised up to 800 °C using the same profile in the case of carbonization at 800 °C, and then it was raised again to 1000 °C or 1200 °C, respectively, at 2 °C·min^{-1} and held for 1 h. The temperature profile of cooling was controlled at 5 °C·min^{-1} from 1000 °C (or 1200 °C) to 800 °C, then 10 °C min^{-1} was set from 800 °C to room temperature (Fig. S2, Supporting Information).

2.2. CNT/C composite fiber manufacturing

Control samples of CNT/C composite fibers without *py*-PDA (without step I) were prepared in a similar way. All processes including phenolic resin infiltration, twisting, curing, and thermal treatment for CNT/C composite fibers were the same as those carried out for the preparation of CNT/*py*-PDA/C composite fibers, with the exclusion of the PDA functionalization. For comparison, the pristine CNT fibers (twisted raw CNTR) and CNT/PDA fibers (twisted PDA functionalized CNTR) were also prepared. It is important to point out that higher concentration of resin solution in this study, is

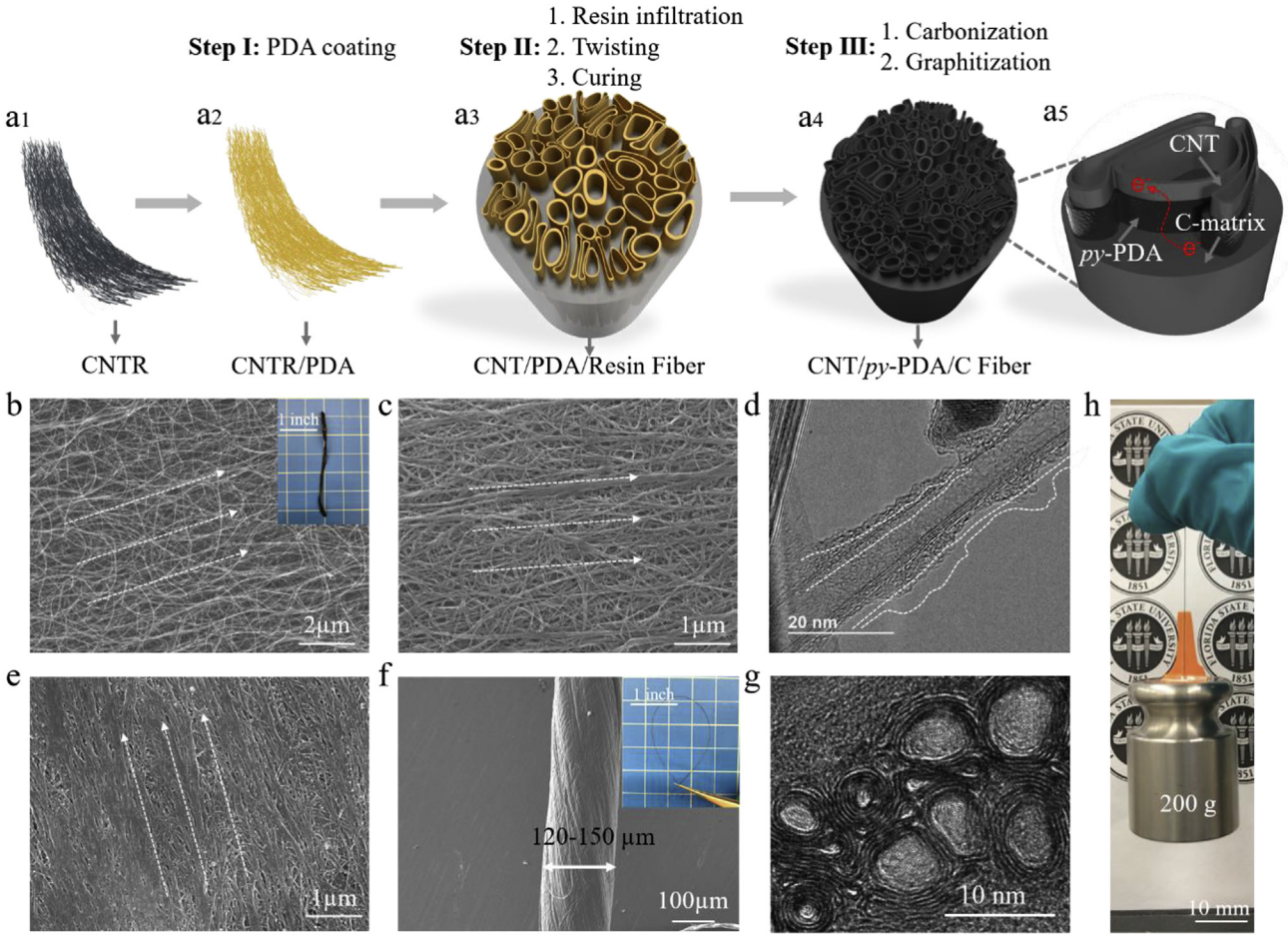

Fig. 1. Manufacturing of CNT/py-PDA/C composite fiber. (a1-a5) Schematic illustrations of the preparation process of the py-PDA/CNT/C composite fiber including three steps: step I-PDA coating (before (a1) and after (a2) coating); step II-resin infiltration, mechanical twisting, and curing (the cross-section of CNT/PDA/Resin fiber in (a3)); step III-thermal treatment at high temperature (the cross-section of CNT/*py*-PDA/C fiber in (a4) and the interface structure in (a5)). (b) Surface morphology of as-received raw CNTR (inset: the digital image of CNTR) with large pores and partial CNT alignment (white arrows show the main alignment direction of CNTs). (c) SEM image of PDA coated CNTR. (d) TEM image of PDA coated CNT with a varied thickness of PDA along CNT longitudinal direction. (e) Surface morphology of CNT/py-PDA/C composite fiber with a dense and aligned structure (white arrows show the main alignment direction of CNTs). (f) The average diameter of as-prepared composite fiber ranging from 120 to 150 μm (inset: digital image shows the flexibility of CNT/py-PDA/C fiber). (g) The cross-section of CNT/py-PDA/C fiber. (h) A weight of 200 g lifted by a CNT/py-PDA/C fiber. (A colour version of this figure can be viewed online.)

assumed to ensure a higher resin content within CNTR (Fig. S1b, Supporting Information); therefore, leading to a better continuous carbon matrix after thermal treatment. However, the increased viscosity is a great concern for the effective infiltration process, and concentrations of greater than 10 wt.% will be explored in the future research.

2.3. CNTR/py-PDA

py-PDA functionalized CNTR (CNTR/*py*-PDA) samples were prepared to investigate the surface morphology. All samples were prepared and carbonized at 1200 °C under identical conditions, except for the different PDA functionalization time (including control sample). Once the PDA functionalized CNTR was dry, a thermal treatment was carried out in an Ar atmosphere (tube furnace, GSL-1600X-OTF, MTI Corporation) using the same temperature profile used for the CNT/*py*-PDA/C composite fibers preparation. Surface morphology of all samples were characterized by AFM.

2.4. Material characterizations

SEM images were obtained using a JOEL JSM-7401F with field-emission gun. TEM images were taken using the JEM-ARM200 cF (Sub-Angstrom Cs Corrected Transmission/Scanning Transmission Electron Microscope from JEOL) at 80 kV allowing for high image contrast without any structural damages. The TEM samples were prepared by peeling and cutting the broken areas of CNTR/PDA and placing them on TEM mesh grids. The thickness of PDA in the vicinity of CNTs was analyzed by the open source software Image J. The resin percentage of CNTR after dipping in various resin solutions was determined by using thermogravimetric analysis (TGA). Focused ion beam (FIB), which is suitable for CNT composite milling without structural damages [44], was used to prepare samples for the characterization of the cross-section of CNT/*py*-PDA/C composite fibers. Mechanical properties were characterized by Dynamic Mechanical Analyzers (DMA, Q800, TA Instruments) with force control of 1 N/min for all samples (gauge length of 10 mm). The average values of ultimate tensile strength, modulus, and failure strain for each sample prepared under different conditions were based on 6–12 trials. Atomic force microscope (AFM, Bruker Inc.) images were taken by Multimode 8 with a Nanoscope V controller. The surface roughness (R_a) was obtained from line scanning profiles of 3–6 lines. Electrical conductivity was tested using the four-probe method with a current source (Keithley 6221) and nanovoltmeter (Keithley 2182A) equipped with an in-house

designed sample holder [45]. The wide-angle X-ray diffraction (WAXD) measurements were obtained on a Bruker NanoSTAR system with an Incoatec IμS microfocus X-ray source operating at 45 kV and 650 μA. The beam was collimated with cross-coupled Göbel mirrors and three pin-hole system, providing a Cu Ka radiation beam ($\lambda = 0.154$ nm) with a beam size about 0.15 mm in full width half maximum (FWHM) at the sample position. The wide-angle diffraction intensity was captured by a Fuji Photo Film image plate and read with a Fuji FLA-7000 scanner. The Raman spectroscopy was carried out on a Renishaw inVia micro-Raman system using a 785 nm excitation wavelength (1.58 eV) diode laser. The DSC results were obtained from TA Instruments Q100 DSC with a 10 °C·min^{-1} heating rate.

3. Results and discussions

3.1. Manufacturing process of CNT/py-PDA/C composite fiber

CNT/*py*-PDA/C composite fibers were prepared through a simple and scalable method – the combination of dip-coating and PIP method (Fig. 1a1-a5) [23,25,37]. The interface engineering was achieved through the dip-coating of PDA followed by thermal treatment conversion of PDA into py-PDA and phenolic resin into the carbon matrix. Therefore, a CNT/*py*-PDA/C composite fiber with *py*-PDA as the interface enhancer was achieved as illustrated in Fig. 1a5. Using *py*-PDA as an interface enhancer for CNT/C composite was manifested by following advantages: (i) the adhesive nature of PDA can introduce a strong bonding between CNTs and phenolic resin through π - π interactions and hydrogen bondings [37,46]; (ii) after carbonization, the strong interface interactions between CNTs and carbon matrix was maintained through physical interlocking effects of *py*-PDA, which can enhance the load transfer efficiency [36,47]; (iii) the py-PDA served as a conductive bridge to minimize the contact resistance between CNTs and carbon matrix [36,37,47]. The latter two advantages were completely different from the effects provided by other polymers or direct covalent bonding explored in the previous CNT/C composites manufacturing [15,20,23,26]. As a result, both mechanical and electrical properties were improved for the CNT/*py*-PDA/C composite fiber after the introduction of *py*-PDA, which served as an adhesive and electron pathway between the CNTs and carbon matrix. Furthermore, since the raw material of CNTR can be mass produced by several manufacturers, including Nanocomp Technologies Inc [48]. and Carbon Solutions, Inc. [49], the reported manufacturing method of combining dip coating and PIP method in this paper is practical and easily scalable, which can take advantages of commercially available CF manufacturing process.

The raw porous CNTR were pre-aligned (Fig. 1b) along longitudinal direction because of the mechanical stretching during the ribbon collection from chemical vapor deposition (CVD) furnace. This porosity of the CNT network was favorable for the PDA coating and phenolic resin infiltration. The PDA aggregated on the surface of CNTs through self-polymerization [37,39] as seen in the SEM and TEM image (Fig. 1c and d) of the morphology of PDA coated CNTR (functionalization time of 60 min). The porous structure was still present after PDA coating (Fig. 1c); however, the thickness of PDA coating was not homogeneous (Fig. 1d), varying from 3 to 12 nm with an average of 7 nm. (Fig. S3, Supporting Information). The following phenolic resin (10 wt.%) infiltration process increased the CNT network density due to the solvent evaporation (Fig. 1e) [50], and the mechanical twisting improved the alignment degree of CNT bundle (Fig. 1e) because of the internal self-stretching [51] (a quantitative comparison of alignment degree between CNTR and composite fibers was discussed later). The final CNT/*py*-PDA/C composite fiber showed a relatively uniform diameter, similar twisting angle (Figs. S4c–f, Supporting Information), and a highly densified structure, as seen in the SEM image in Fig. 1f, with a diameter of greater than 100 μm. Fig. 1g shows the cross section of CNT/*py*-PDA/C composite fiber (sample was prepared by FIB). Compared to previous results in literature [13,14,23,24], the CNT/*py*-PDA/C composite fiber had a larger diameter, and the length is only constrained by the length of the raw CNTRs. A CNTR and a roll of CNT/*py*-PDA/C composite fiber measuring 1.5 m long is displayed in Figs. S4a–b (Supporting Information). Even after thermal treatment at high temperature, the composite fibers remained mechanically flexible (Fig. 1f inset, Fig. S4 and Video S1, Supporting Information) and strong (Fig. 1h, Video S2, Supporting Information).

Supplementary video related to this article can be found at https://doi.org/10.1016/j.carbon.2018.12.091

3.2. The optimization of experimental conditions

The mechanical and electrical properties of CNT/C and CNT/*py*-PDA/C composite fibers were systematically investigated by varying processing parameters, including the concentration (wt.%) of phenolic resin solution, PDA coating time (t), and the temperature of thermal treatment (T). Infiltrating sufficient polymer carbon precursor into the CNT network is important to ensure that a dense and continuous carbon matrix can be achieved after high temperature carbonization. As a result, the carbon matrix filled the voids, making the final CNT/C composite fiber dense. On the other hand, a more efficient load transfer may be achieved from the continuous carbon matrix, which interconnected all CNTs together within the network. In this study, three different concentrations (3, 5, and 10 wt.%) of phenolic resin were investigated, and their corresponding composite fibers were referred to as CNT/C-X (X is the weight percent of phenolic resin solution). The surface morphology depicted in Fig. 2a–c shows a dense packing structure of CNTs and carbon matrix. These morphologies were achieved for all three studied cases of CNT/C-3 (3 wt.%, Fig. 2a), CNT/C-5 (5 wt.%, Fig. 2b), and CNT/C-10 (10 wt.%, Fig. 2c), as compared to raw CNTR (Fig. 1b). As shown in Fig. 2c, a denser and more continuous structure was achieved by CNT/C-10 composite fiber. Since the concentration of phenolic resin solution increased, more polymer carbon precursor was infiltrated into the CNT networks. Consequently, the CNT/C-10 composite fiber was expected and experimentally verified to demonstrate greater properties than the other two counterparts of CNT/C-3 and CNT/C-5 samples due to the better interconnections between CNTs and carbon matrix. This assumption was verified by the following mechanical and electrical property investigations. Therefore, 10 wt.% of phenolic resin solution was used in production of CNT/*py*-PDA/C composite fibers to guarantee the dense and continuous carbon matrix.

The typical stress-strain curves of CNT/C@T1200 composite fibers (thermal treatment at 1200 °C) are plotted in Fig. 2d. Based on the observed surface morphology and microstructure analysis of SEM images in Fig. 2a–c, the CNT/C-10@T1200 was found to perform better mechanically as compared to the other two of CNT/C-3@T1200 and CNT/C-5@T1200 fibers. This was the evidence that a dense and continuous carbon matrix enhanced the interconnections between neighboring CNTs.

This research also attempted to further improve the mechanical properties of CNT/C composite fiber by thermal treatment, which has significant effects on the microstructure of carbon matrix [52]. Therefore, three thermal treatment conditions of 800 °C, 1000 °C, and 1200 °C were used to carbonize phenolic resin. The stress-strain curves of CNT/C@T800 and CNT/C@T1000 composite fibers were plotted in Fig. S5 (Supporting Information, detail values can be found in Table S1). Compared to CNT/C@T800 and CNT/C@T1000

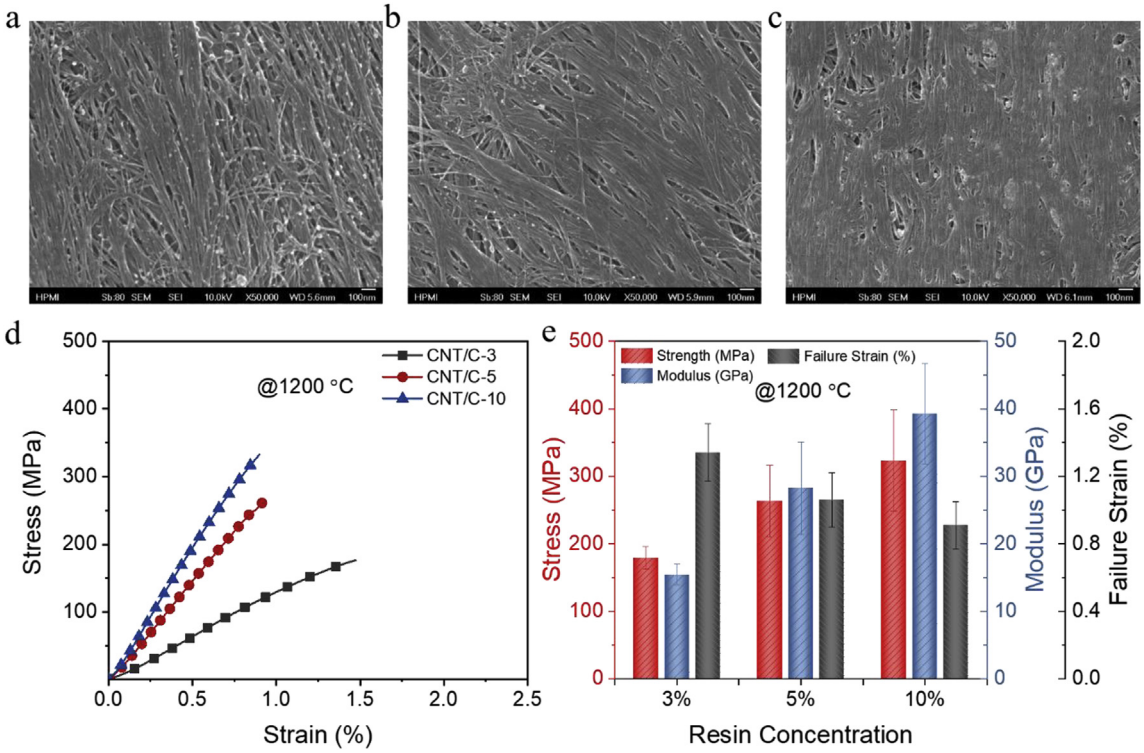

Fig. 2. Surface morphology and mechanical properties of CNT/C@T1200 composite fibers. (a–c) Surface microstructures of samples prepared by using (a) 3 wt.% (CNT/C-3@T1200), (b) 5 wt.% (CNT/C-5@T1200), and (c) 10 wt.% (CNT/C-10@T1200) of phenolic resin solution. (d–e) The stress-strain curves CNT/C composite fibers and their corresponding averaged values of ultimate tensile strength, modulus, and failure strain. (A colour version of this figure can be viewed online.)

composite fibers using a fixed wt.% of phenolic resin solution (e.g. 10 wt.%), higher tensile strength and modulus were achieved for samples of CNT/C-10@T1200, as shown in Fig. 2e, reaching 323 MPa and 39.2 GPa, respectively. Generally, high temperature treatment can graphitize the carbon matrix, resulting in a strong matrix, yielding better mechanical performance [23,33]. Thus, in terms of wt.% of phenolic resin solution and thermal treatment temperature, the mechanical performance of CNT/C-10@T1200 composite fiber was much better than that of CNT/C-3@T800 composite fiber. Based on these results, 10 wt.% of phenolic resin solution and thermal treatment at 1200 °C were used to prepare CNT/*py*-PDA/C composite fibers to investigate the effects of *py*-PDA functionalization. Additionally, a decreased failure strain was observed for samples carbonized at a higher temperature (Figs. S3b and S3d, Table S1, Supporting Information) due to the microstructure difference of nanocrystalline carbon matrix [23].

3.3. The effects introduced by py-PDA

The effects of PDA coating time (t) on the mechanical properties of composite fibers were also investigated (referred to as CNT/*py*-PDA/C@tY, with Y indicating the coating time in minutes). Similar surface morphologies were observed for samples of CNT/*py*-PDA/C composite fibers prepared with different functionalization time from 5 to 120 min (Fig. S6, Supporting Information). As a result, the introduction of PDA on CNTR seemed not to exert any negative effects on the following phenolic resin infiltration process. Fig. 3a shows the tensile strength of CNT/*py*-PDA/C@T1200 fibers simultaneously increased with the extension of PDA functionalization time from 5 to 60 min. However, further extending PDA coating time (120 min) did not further increase the tensile strength. Instead, a slight decrease was observed, which may be ascribed to the weaker strength of *py*-PDA itself as compared to CNTs or carbon matrix [36].

For comparison, the ultimate tensile strength, modulus, and failure strain were extracted from the curves in Fig. 3a and plotted in Fig. 3b (detailed values were listed in Table S2, Supporting Information). In this study, for the CNT/*py*-PDA/C@t60-T1200 composite fiber, both modulus and tensile strength reached the optimum of 85 GPa and 727 MPa, respectively (the highest strength of 841 MPa and modulus of 105 GPa were observed). Overall, CNT/*py*-PDA/C@t60-T1200 composite fibers showed better mechanical performance than their counterparts of CNT/C@1200 composite fibers: more than double in terms of tensile strength and modulus. The strength is much higher than that of carbon fiber-based C/C composites, which are usually in the range of 100–250 MPa [53–55]. When compared to the pristine CNT fiber (without py-PDA functionalization and carbon matrix infiltration, Fig. S5e, Supporting Information), or PDA functionalized CNT fiber (without carbon matrix infiltration, Fig. S5e, Supporting Information) and other reported CNT or graphene reinforced C/C composites [3,13,14], this improved mechanical performance is still significant. Additionally, the mechanical properties observed were even better than that of biomaterials derived nanocarbon fibers, which were treated at an extremely high temperature up to 2800 °C (such a high temperature treatment may also be helpful for our case, but it is energy-insufficient) [52]. Furthermore, the failure strain of CNT/*py*-PDA/C@t60-T1200 composite fiber, reaching $1.01 \pm 0.17\%$, was also observed slightly higher than that of CNT/C@1200 fiber, $0.91 \pm 0.14\%$.

The improvements of mechanical properties could be ascribed to the introduction of *py*-PDA as an interface enhancer [36,37,47], which can result in strong interactions between CNTs and carbon matrix, leading to a better load transfer among neighboring CNTs. Based on the morphology of PDA coated CNTs (Fig. S3, Supporting Information), a rough surface of *py*-PDA in the vicinity of CNTs was

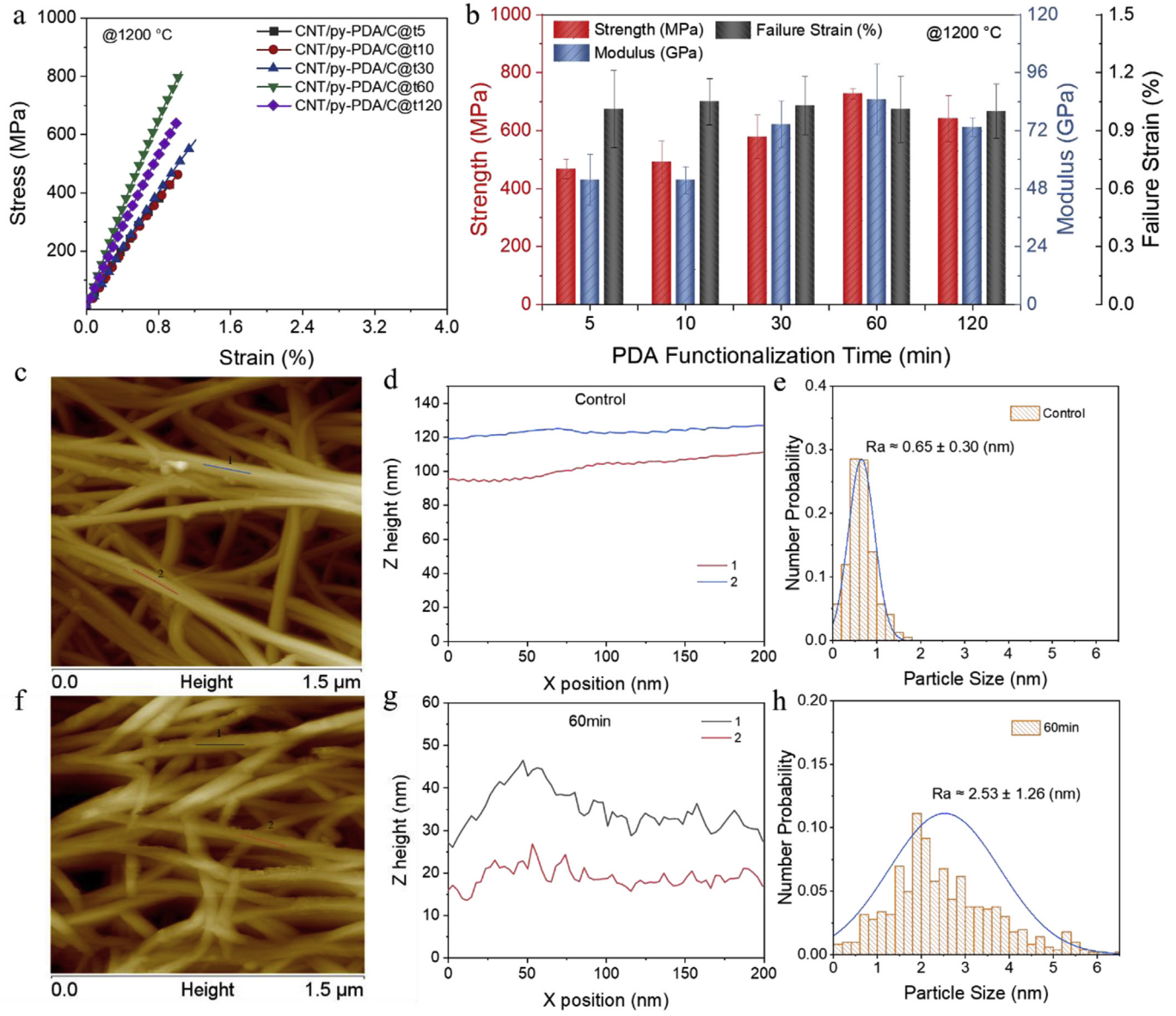

Fig. 3. Mechanical properties of CNT/*py*-PDA/C@T1200 composite fibers with different PDA functionalization time of 5, 10, 30, 60, and 120 min. (a) The stress-strain curves and (b) their corresponding averaged values of tensile strength, modulus, and failure strain. (c–h) Surface morphology and characteristic roughness of (c–e) CNTR and (f–h) CNTR/*py*-PDA by AFM including survey images (c and f), representative scanning line profiles (d and g), and the histogram distribution of surface roughness (e and h). (A colour version of this figure can be viewed online.)

expected after carbonization. Thus, the AFM surface morphology results of both raw CNTR (without *py*-PDA) and functionalized CNTR with different coating time (with *py*-PDA) were collected, as shown in Fig. 3c–h and Fig. S7 (Supporting Information). The typical surface morphology of CNTR and CNTR/*py*-PDA are displayed in Fig. 3c and f, and the two representative scanning line profiles plotted along the CNT surface are provided in Fig. 3d and g. Based on the definition of surface roughness (R_a) (excluding the baseline of CNTs themselves), the CNTR showed a value of R_a as small as 0.65 nm (Fig. 3e). However, the R_a of CNTR/*py*-PDA gradually increased from 1.54 nm (Fig. S7c, Supporting Information) to 2.53 nm (Fig. 4f) with the increase of functionalization time from 5 to 60 min. Results from AFM data confirmed the hierarchical structure of *py*-PDA on the surface of CNTs after carbonization [36]. Additionally, the increasing R_a correlated with the improved mechanical properties of CNT/*py*-PDA/C composite fiber. Therefore, the increased surface roughness was beneficial for physical interaction such as interlocking between CNTs and carbon matrix. The hierarchical structure of pyrolyzed PDA was also reported to enhance interactions between graphene nanosheets [36,47,56]. A slight decrease of R_a for the case of CNTR/*py*-PDA at 120 min (Fig. S7), which may result from the excessive conformal thickness of PDA, explained the decreased tensile strength of CNT/*py*-PDA/C@t120-T1200 composite fiber. These findings are summarized in Fig. 3b.

Due to the incorporation of PDA, the potential effects of thermal treatment temperature on the mechanical properties of CNT/*py*-PDA/C@T800, CNT/*py*-PDA/C@T1000, and CNT/*py*-PDA/C@T1200composite fibers were studied. As expected, no negative effects were observed from the presence of *py*-PDA. The same trend of temperature effects was found for both CNT/C and CNT/*py*-PDA/C composite fibers (Fig. 3b). As the carbonization temperature was

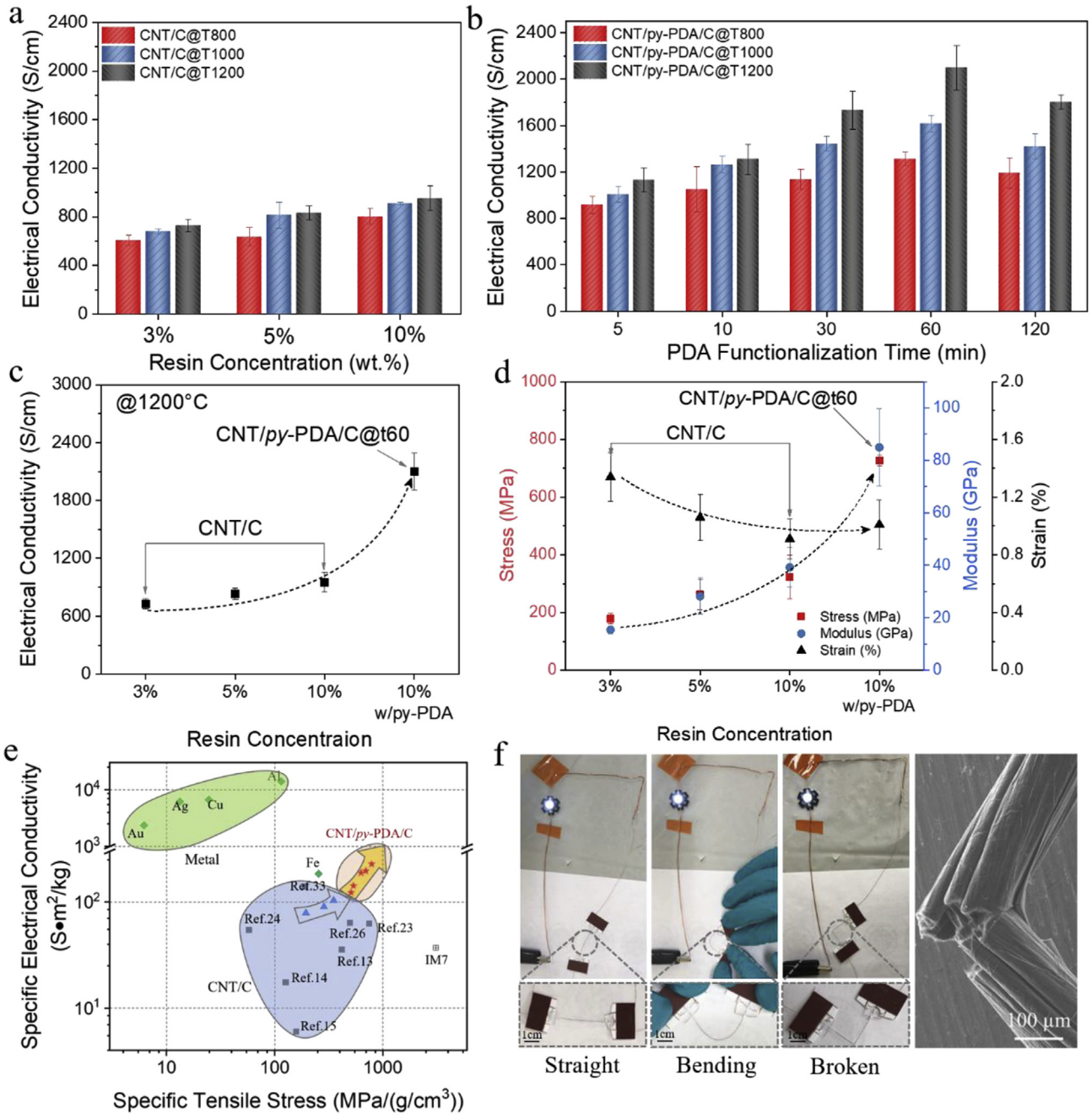

Fig. 4. Electrical conductivity of CNT/*py*-PDA/C composite fibers. (a) Effects of the concentration of phenolic resin solution and thermal treatment temperature on the conductivity of CNT/C composite fibers. (b) Effects of PDA functionalization time and thermal treatment temperature on the conductivity of CNT/*py*-PDA/C composite fibers. (c–e) The comparison of the electrical and mechanical performance between our CNT/*py*-PDA/C and CNT/C composite fibers, and results from literature. (c) The improvement of electrical conductivity and (d) tensile strength, modulus, and failure strain of CNT/*py*-PDA/C and CNT/C composite fibers (the dashed arrow is a guideline for eyes). (e) Comparison overview of our results of CNT/*py*-PDA/C composite fiber versus results from literature. (f) The demonstration of CNT/*py*-PDA/C composite fiber being used as a flexible non-metal conductor. (A colour version of this figure can be viewed online.)

increased so did the mechanical performance (Fig. S8, Supporting Information). For example, the corresponding tensile strengths of 565 MPa and 471 MPa were achieved for CNT/*py*-PDA/C@t60-T1000 and CNT/*py*-PDA/C@t60-T800 composite fibers (Table S2, Supporting Information). Nevertheless, these values were much higher than that of control CNT/C composite fibers carbonized at the same temperature, 296 MPa for CNT/C@1000 and 194 MPa for CNT/C@800, respectively (Table S1, Supporting Information).

3.4. The improved electrical and mechanical properties

Another key application of CNT/C composites is use of its potential high electrical conductivity. This property was investigated for CNT/C and CNT/*py*-PDA/C composite fibers. For CNT/C composite fibers, Fig. 4a shows the effects of the phenolic resin concentration and the thermal treatment temperature on the electrical conductivity. Under same thermal treatment temperature, higher conductivity was found for samples prepared using higher wt.% of phenolic resin. This trend is associated with the improvements

discovered in mechanical performance (Fig. 2e). As previously discussed, when the higher concentration of phenolic resin solution was used, dense and continuous carbon matrix was achieved within CNT networks after carbonization. Therefore, more conductive pathways were rebuilt among neighboring CNTs, which can explain the trend of increased electrical conductivity of CNT/C-3, CNT/C-5, and CNT/C-10. As the carbonization temperature raised from 800 to 1200 °C, the highest electrical conductivity was achieved for the CNT/C-10@T1200 composite fiber, measuring up to 9.5×10^2 S cm^{-1}. This value is similar to that of pristine CNT fiber reported in the range of $(9–10) \times 10^2$ S cm^{-1} (Table S3, Supporting Information). For comparison, the conductivity of CNT/C-3@T1200 was 7.2×10^2 S cm^{-1}. After the introduction of *py*-PDA, all CNT/*py*-PDA/C@T1200 composite fibers showed a higher conductivity than that of CNT/C@1200 composite fiber, as shown in Fig. 4b. A significant enhancement of conductivity was recorded for CNT/*py*-PDA/C@t60-T1200 composite fibers, reaching 2.1×10^3 S cm^{-1} (Fig. 4b), which is the highest value reported for CNT/C composites based on literature survey (Fig. 4e). This value was comparable to the pitch-based highly conductive carbon fiber [57]. The reason of such a great improvement of electrical conductivity for CNT/*py*-PDA/C composite fibers could be accredited to pyrolytic carbon of *py*-PDA, which may serve as conductive pathways between CNTs and carbon matrix [37,58]. As a comparison, CNT/PDA fiber (just by twisting PDA functionalized CNTR without any further thermal treatment) had a conductivity in the range of only $(4–5) \times 10^2$ S cm^{-1} (Table S3, Supporting Information). Thus, the contact resistance among neighboring CNTs and between CNT and C matrix can be minimized when the optimal thickness of *py*-PDA coating was achieved (coating time of 60 min in this study). For the optimal case of CNT/*py*-PDA/C@t60-T1200 composite fiber, a continuous and rough film of *py*-PDA was possibly formed acting as an interface enhancer among CNTs and carbon matrix (Fig. 1a5). This appears to result in both electrically conductive pathways for conductivity enhancement (Fig. 4b) and physical interlocking for mechanical improvement (Fig. 3b). For the cases of functionalization time of less than 60 min (5, 10 and 30 min in this study), the lower conductivity could result from the less conductive pathways due to non-continuity of the *py*-PDA. When the functionalization time was more than 60 min (120 min in this study), the enhancement of conductivity from *py*-PDA induced contact resistance decreased suggesting *py*-PDA saturation. Thus, no further conductivity improvements were observed (Fig. 4b). The slight decrease of conductivity of CNT/*py*-PDA/C@t120-T1200 composite fiber may be due to the over coating of *py*-PDA, since its conductivity is much poorer than that of CNT [11,41,42].

Overall, by controlling the concentration of phenolic resin solution, thermal treatment temperature, and the unique functionalization of *py*-PDA, properties including electrical and mechanical, were improved. An overview of comparisons between CNT/C and CNT/*py*-PDA/C composite fibers, including conductivity, ultimate tensile strength, modulus, and failure strain is summarized in Fig. 4c and d. A steady increase of conductivity, tensile strength, and modulus of CNT/C@T1200 composite fibers were observed as the concentration of phenolic resin solution went from 3 to 10 wt.%. Moreover, significant improvements on both mechanical and electrical performance were achieved in the CNT/*py*-PDA/C@t60-T1200 composite fibers. The failure strain was even higher than that of CNT/C@1200 composite fiber. Compared to the results reported in literature, our CNT/*py*-PDA/C composite fiber showed very competitive characteristics in both mechanical and electrical performance with a large sample size. More importantly, the fabrication method reported in this study could shed light on the future C/C composite manufacturing by emphasizing interface property engineering. Considering the density of 0.92–1.14 g cm^{-3} for CNT/C and CNT/*py*-PDA/C composite fibers, the fibers produced in this study achieved the highest specific tensile strength and electrical conductivity in the field of CNT/C composites, as shown in the plot of Fig. 4e (Table S3, Supporting Information). This is significantly advantageous for applications where weight is of a great concern for cost reduction. When being used as a flexible non-metal conductor, our CNT/*py*-PDA/C composite fiber showed advantages of moderate specific conductivity and high specific tensile strength compared to conventional metal conductors [59]. A demonstration of a LED illuminated by a *py*-PDA/CNT/C composite fiber under three different modes – straight, bending, and fractured – is shown in Fig. 4f (Video S3 and Video S4, Supporting Information). While the fiber underwent mechanical bending, no obvious change for the intensity of LED was observed. Even after the fiber was fractured (partially tore apart, SEM image in Fig. 4f), the LED was still illuminated. This may be another indication of the resilient interactions between CNTs and CNT/C matrix with *py*-PDA/CNT/C composite fibers.

Supplementary video related to this article can be found at https://doi.org/10.1016/j.carbon.2018.12.091

3.5. The structural and chemical investigations

To further verify the effects of *py*-PDA on CNT microstructures and properties, more detailed structural characterizations were performed. The XRD patterns were collected for CNT/C and CNT/*py*-PDA/C composite fibers to obtain the nanocrystalline structure. For comparison, Fig. 5a shows characterization results of raw CNTR and heated CNTR (at 1200 °C). One characteristic peak at 25.5° was attributed to the lattice plane of (002) [14,29]. Table 1 lists the calculated structural parameters of (002) peak of these samples. Using the Bragg equation, d_{002} (interlayer spacing) was extracted. Similarly, the L_c (stacking height) was obtained according to the Scherrer equation. The d_{002} (0.340 nm) and L_c (2.711 nm) of raw CNTR were in agreement with the values found in literature [60]. The decreased d_{002} and enlarged L_c of heated CNTR may result from removing amorphous carbon from CNTs by thermal treatment. After the carbon matrix was introduced, a widened (002) peak was observed for both CNT/C@T800 and CNT/*py*-PDA/C@t60-T800 composite fibers. However, as thermal treatment temperature increased to 1200 °C, a sharp FWHM and decreased d_{002} was recorded (Table 1), which indicated the graphitization of carbon matrix, and the healing of CNTs as similar as the case of heated CNTR. Larger L_c may also explain the higher mechanical properties of CNT/*py*-PDA/C composite fiber than their counterparts of CNT/C samples at same thermal treatment temperature. The azimuthal scans around d_{002} in Fig. 5b allowed insights into the structural difference of samples in terms of CNT alignment. As expected, compared to CNTR, better CNT alignment was achieved, which is consistent with the surface morphology (Fig. 1e) and beneficial for both electrical and mechanical properties [61,62], by fiber manually twisting process. This was verified by the higher ratio of the maximum intensity (90°, the longitudinal direction of fibers) versus minimum intensity [44].

Fig. 5c shows the comparison of Raman spectra of CNTR, CNT/C and CNT/*py*-PDA/C samples. The prominent G band peak indicates the high nanocrystalline structure. After thermal treatment, the ratio of I_G/I_D (a characteristic of defect density of carbon materials: the higher I_G/I_D value indicated a better developed graphitic structure [14]) of heated CNTR increased to 16.13, as compared to 15.63 of CNTR. This slight improvement of structure agreed with the data in Table 1. For CNT/C10@800 composite fibers, most amorphous carbon was from carbon matrix resin, resulting in more defects with low I_G/I_D value of 4.95, compared to 16.13 of heated CNTR. For the case of CNT/*py*-PDA/C@t60-T800 samples, the even

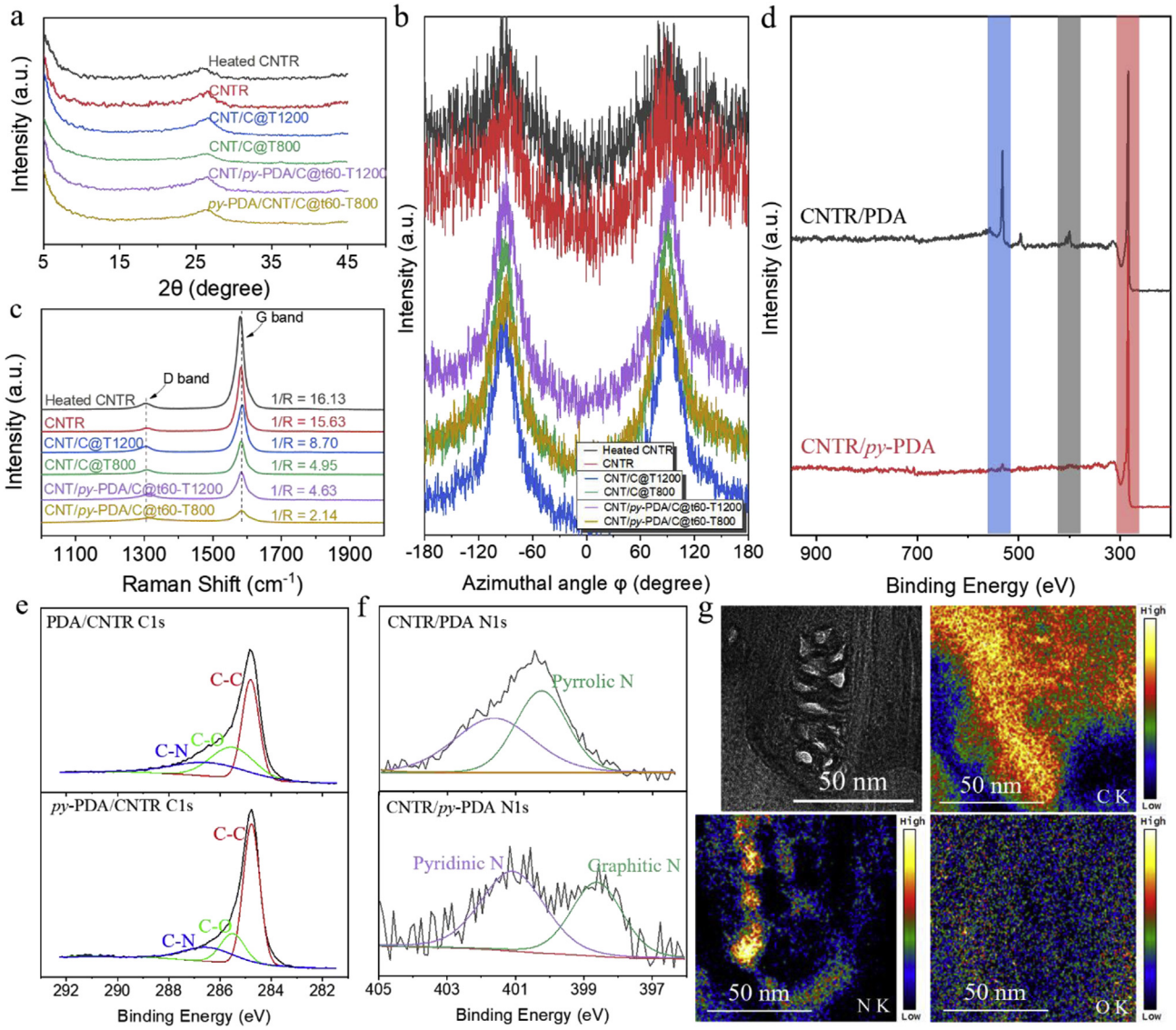

Fig. 5. Structural and composition characterizations of CNT/C and CNT/*py*-PDA/C composite fibers. (a) XRD patterns of CNT/C and CNT/*py*-PDA/C fibers carbonized at both low (800 °C) and high (1200 °C) temperature. Data for CNTR and heated CNTR (at 1200 °C) were collected as a control. Their corresponding azimuthal scans (b) and Raman spectra (c) of all samples in (a) were plotted. (d) XPS spectra of CNTR/PDA and CNTR/*py*-PDA including (e) C1s and (f) N1s spectra. (g) Elastic and EFTEM of a cross-section of CNT/py-PDA/C composite fiber. (A colour version of this figure can be viewed online.)

Table 1
The structural parameters of different samples calculated from WAXD based on Bragg equation and Scherrer equation.

Sample	2θ (degree)	FWHM (degree)	d(002)[a] (nm)	L_c(002)[b] (nm)
CNTR	25.36	3.341	0.351	2.707
Heated CNTR	25.91	2.782	0.343	3.254
CNT/C@T800	25.55	3.080	0.348	2.938
CNT/C@T1000	25.68	2.644	0.346	3.423
CNT/C@T1200	25.92	2.290	0.343	3.954
CNT/*py*-PDA/C@T800	25.24	3.023	0.352	2.991
CNT/*py*-PDA/C@T1000	25.76	2.465	0.345	3.672
CNT/*py*-PDA/C@T1200	25.87	2.118	0.344	4.274

[a] $d_{002} = \lambda/(2\sin(\theta_{002}))$, where $\lambda = 0.154$ is the wavelength of X-ray, θ_{002} is the peak position of (002) peak.

[b] $L_c = \lambda/(\beta\cos(\theta_{002}))$, where β is the FWHM. β is extracted from the non-linear curve fit (Gaussian) of the original peak. Very good agreement between fitting and original peak was observed as shown in Fig. S9 (Supporting Information) with an Adj. R-Square higher than 0.9500.

lower I_G/I_D value may be ascribed to the less crystalline structure of *py*-PDA [36].

Nevertheless, increasing the thermal treatment temperature can possibly further graphitize the *py*-PDA and carbon matrix, reaching high I_G/I_D values of 8.70 and 4.63 for CNT/C@1200 and CNT/*py*-PDA/C@t60-T1200 composite fibers, respectively. This trend of I_G/I_D value corresponded to the increase of L_c(002) for each case (Table 1). The successful introduction of *py*-PDA was further verified by XPS C1s and N1s spectra (Fig. 5d–f) of CNTR/PDA and CNTR/*py*-PDA (at 1200 °C). Three representative peaks of C-C bonding at 284.8 eV, C-O bonding at 285.5 eV, and C-N bonding at 286.5 eV were seen in the deconvoluted C1s spectra (Fig. 5e) [37,63]. After thermal treatment at 1200 °C, the relative peak intensity of C-O and C-N significantly decreased (Fig. 5d and e) with a decrease of atomic content of oxygen (O) and nitrogen (N) (Table S4, Supporting Information) due to the pyrolysis of PDA to *py*-PDA. Interestingly, the deconvoluted N1s peak spectra of CNTR/*py*-PDA revealed a strong graphitic N at 401 eV as compared to that

of CNT/PDA, which indicated that PDA was completely pyrolyzed into N doped carbon (*py*-PDA). Therefore, carrier mobility can be improved due to the heterogeneous doping of nitrogen, so the *py*-PDA can serve as conductive pathway among CNTs and carbon matrix, which is beneficial for the enhancement of conductivity of CNT/*py*-PDA/C composite fibers. The elastic and EFTEM images of the cross-section area of CNT/*py*-PDA/C are displayed in Fig. 5g. A clear pattern of N was shown in the vicinity of a CNT bundle, which indicates the well-controlled interface engineering of *py*-PDA among CNTs and carbon matrix.

4. Conclusions

In summary, we reported a scalable method for CNT/C composite fiber manufacturing through the combination of controlling the concentration of phenolic resin solution, mechanical twisting, thermal treatment temperature, and the unique introduction of *py*-PDA as an interface enhancer between CNTs and carbon matrix. The achieved significant improvements of CNT/*py*-PDA/C@t60-T1200 composite fiber including both mechanical (727 MPa) and electrical (2.1×10^3 S cm^{-1}) performance surpassed those of control CNT/C composite fibers (323 MPa and 9.5×10^2 S cm-1, respectively) and results from literature. Such high integrated properties using this method is advantageous for applications where high thermal stability is required, which usually cannot be satisfied using conventional organic polymer cross-linking or chemical doping. The as-prepared CNT/*py*-PDA/C composite fibers were still flexible and bendable. These integrated characteristics of CNT/*py*-PDA/C composite fibers may enable potential applications ranging from electronic devices, including flexible, wearable, and portable sensors, supercapacitors, and batteries, to structural materials where high specific strength and specific conductivity are of great interest.

Acknowledgment

This work was partially supported by AFOSR FA9550-17-1-0005. Songlin Zhang also thanks Yinnan Zhang for the support and helpful suggestions on schematic drawing, and the financial support from China Scholarship Council (CSC no. 201506630022).

Appendix A. Supplementary data

Supplementary data to this article can be found online at https://doi.org/10.1016/j.carbon.2018.12.091.

References

[1] H.G. Maahs, Carbon-carbon Composites: Emerging Materials for Hypersonic Flight, 1989. https://ntrs.nasa.gov/search.jsp?R=19900016764. (Accessed 10 November 2018).
[2] E. Savage, Carbon-carbon Composites, Springer Science & Business Media, 2012.
[3] G. Xin, T. Yao, H. Sun, S.M. Scott, D. Shao, G. Wang, et al., Highly thermally conductive and mechanically strong graphene fibers, Science 349 (6252) (2015) 1083–1087.
[4] L. Kurzepa, A. Lekawa-Raus, J. Patmore, K. Koziol, Replacing copper wires with carbon nanotube wires in electrical transformers, Adv. Funct. Mater. 24 (5) (2014) 619–624.
[5] S. Chand, Review carbon fibers for composites, J. Mater. Sci. 35 (6) (2000) 1303–1313.
[6] X. Huang, Fabrication and properties of carbon fibers, Materials 2 (4) (2009) 2369.
[7] Z. Li, Z. Liu, H. Sun, C. Gao, Superstructured assembly of nanocarbons: fullerenes, nanotubes, and graphene, Chem. Rev. 115 (15) (2015) 7046–7117.
[8] D. Janas, K.K. Koziol, Carbon nanotube fibers and films: synthesis, applications and perspectives of the direct-spinning method, Nanoscale 8 (47) (2016) 19475–19490.
[9] J. Di, X. Zhang, Z. Yong, Y. Zhang, D. Li, R. Li, et al., Carbon-nanotube fibers for wearable devices and smart textiles, Adv. Mater. 28 (47) (2016) 10529–10538.
[10] W. Lu, M. Zu, J.H. Byun, B.S. Kim, T.W. Chou, State of the art of carbon nanotube fibers: opportunities and challenges, Adv. Mater. 24 (14) (2012) 1805–1833.
[11] Q.W. Li, Y. Li, X.F. Zhang, S.B. Chikkannanavar, Y.H. Zhao, A.M. Dangelewicz, et al., Structure-dependent electrical properties of carbon nanotube fibers, Adv. Mater. 19 (20) (2007) 3358–3363.
[12] T.V. Sreekumar, T. Liu, B.G. Min, H. Guo, S. Kumar, R.H. Hauge, et al., Polyacrylonitrile single-walled carbon nanotube composite fibers, Adv. Mater. 16 (1) (2004) 58–61.
[13] Z. Zhou, X. Wang, S. Faraji, P.D. Bradford, Q. Li, Y. Zhu, Mechanical and electrical properties of aligned carbon nanotube/carbon matrix composites, Carbon 75 (2014) 307–313.
[14] Y. Jin, Y. Zhang, Q. Zhang, R. Zhang, P. Li, W. Qian, et al., Multi-walled carbon nanotube-based carbon/carbon composites with three-dimensional network structures, Nanoscale 5 (13) (2013) 6181–6186.
[15] X. Lin, W. Zhao, W. Zhou, P. Liu, S. Luo, H. Wei, et al., Epitaxial growth of aligned and continuous carbon nanofibers from carbon nanotubes, ACS Nano 11 (2) (2017) 1257–1263.
[16] R. Djugum, K. Sharp, The fabrication and performance of C/C composites impregnated with TaC filler, Carbon 115 (2017) 105–115.
[17] X. Zhang, X. Li, G. Yuan, Z. Dong, G. Ma, B. Rand, Large diameter pitch-based graphite fiber reinforced unidirectional carbon/carbon composites with high thermal conductivity densified by chemical vapor infiltration, Carbon 114 (2017) 59–69.
[18] H. Khoshnevis, S.M. Mint, E. Yedinak, T.Q. Tran, A. Zadhoush, M. Youssefi, et al., Super high-rate fabrication of high-purity carbon nanotube aerogels from floating catalyst method for oil spill cleaning, Chem. Phys. Lett. 693 (2018) 146–151.
[19] P. Liu, A.L. Cottrill, D. Kozawa, V.B. Koman, D. Parviz, A.T. Liu, et al., Emerging trends in 2D nanotechnology that are redefining our understanding of "Nanocomposites", Nano Today 21 (2018) 18–40.
[20] J. Lee, T. Kim, Y. Jung, K. Jung, J. Park, D.M. Lee, et al., High-strength carbon nanotube/carbon composite fibers via chemical vapor infiltration, Nanoscale 8 (45) (2016) 18972–18979.
[21] S. Faraji, O. Yildiz, C. Rost, K. Stano, N. Farahbakhsh, Y. Zhu, et al., Radial growth of multi-walled carbon nanotubes in aligned sheets through cyclic carbon deposition and graphitization, Carbon 111 (2017) 411–418.
[22] S. Faraji, K. Stano, C. Rost, J.-P. Maria, Y. Zhu, P.D. Bradford, Structural annealing of carbon coated aligned multi-walled carbon nanotube sheets, Carbon 79 (2014) 113–122.
[23] Y. Han, S. Li, F. Chen, T. Zhao, Multi-scale alignment construction for strong and conductive carbon nanotube/carbon composites, Materials Today Communications 6 (2016) 56–68.
[24] X. Li, L. Ci, S. Kar, C. Soldano, S.J. Kilpatrick, P.M. Ajayan, Densified aligned carbon nanotube films via vapor phase infiltration of carbon, Carbon 45 (4) (2007) 847–851.
[25] J.G. Park, N.G. Yun, Y.B. Park, R. Liang, L. Lumata, J.S. Brooks, et al., Single-walled carbon nanotube buckypaper and mesophase pitch carbon/carbon composites, Carbon 48 (15) (2010) 4276–4282.
[26] V. Thiagarajan, X. Wang, P.D. Bradford, Y.T. Zhu, F.G. Yuan, Stabilizing carbon nanotube yarns using chemical vapor infiltration, Compos. Sci. Technol. 90 (2014) 82–87.
[27] M. Scholz, Y. Hayashi, V. Khavrus, D. Chujo, H. Inoue, M. Hada, et al., Resistance-heating of carbon nanotube yarns in different atmospheres, Carbon 133 (2018) 232–238.
[28] S.Y. Moon, W.S. Kim, High mechanical properties of super aligned carbon nanocomposite by polyurethane based crosslinking molecules, Compos. Sci. Technol. 161 (2018) 100–106.
[29] J. Liu, W. Gong, Y. Yao, Q. Li, J. Jiang, Y. Wang, et al., Strengthening carbon nanotube fibers with semi-crystallized polyvinyl alcohol and hot-stretching, Compos. Sci. Technol. 164 (2018) 290–295.
[30] S. Ryu, Y. Lee, J.W. Hwang, S. Hong, C. Kim, T.G. Park, et al., High-strength carbon nanotube fibers fabricated by infiltration and curing of mussel-inspired catecholamine polymer, Adv. Mater. 23 (17) (2011) 1971–1975.
[31] S. Wan, S. Fang, L. Jiang, Q. Cheng, R.H. Baughman, Strong, conductive, foldable graphene sheets by sequential ionic and pi bridging, Adv. Mater. 30 (36) (2018) 1802733.
[32] Y. Zhang, J. Peng, M. Li, E. Saiz, S.E. Wolf, Q. Cheng, Bioinspired supertough graphene fiber through sequential interfacial interactions, ACS Nano 12 (9) (2018) 8901–8908.
[33] X. Zhang, L. Yang, H. Liu, Enhancements in mechanical and electrical properties of carbon nanotube films by SiC and C matrix bridging, J. Mater. Sci. 53 (15) (2018) 11027–11037.
[34] N. Zhao, M. Yang, Q. Zhao, W. Gao, T. Xie, H. Bai, Superstretchable nacre-mimetic graphene/poly(vinyl alcohol) composite film based on interfacial architectural engineering, ACS Nano 11 (5) (2017) 4777–4784.
[35] Y. Cheng, J. Peng, H. Xu, Q. Cheng, Glycera-Inspired synergistic interfacial interactions for constructing ultrastrong graphene-based nanocomposites, Adv. Funct. Mater. (2018) 1800924.
[36] T. Ma, H.L. Gao, H.P. Cong, H.B. Yao, L. Wu, Z.Y. Yu, et al., A bioinspired interface design for improving the strength and electrical conductivity of graphene-based fibers, Adv. Mater. 30 (15) (2018) 1706435.
[37] S. Ryu, J.B. Chou, K. Lee, D. Lee, S.H. Hong, R. Zhao, et al., Direct insulation-to-conduction transformation of adhesive catecholamine for simultaneous increases of electrical conductivity and mechanical strength of CNT fibers, Adv.

Mater. 27 (21) (2015) 3250–3255.
[38] H. Kim, R. Jalili, G.M. Spinks, G.G. Wallace, S.J. Kim, High-strength graphene and polyacrylonitrile composite fiber enhanced by surface coating with polydopamine, Compos. Sci. Technol. 149 (2017) 280–285.
[39] Y. Liu, K. Ai, L. Lu, Polydopamine and its derivative materials: synthesis and promising applications in energy, environmental, and biomedical fields, Chem. Rev. 114 (9) (2014) 5057–5115.
[40] X. Yu, H. Fan, Y. Liu, Z. Shi, Z. Jin, Characterization of carbonized polydopamine nanoparticles suggests ordered supramolecular structure of polydopamine, Langmuir 30 (19) (2014) 5497–5505.
[41] R. Li, K. Parvez, F. Hinkel, X. Feng, K. Müllen, Bioinspired wafer-scale production of highly stretchable carbon films for transparent conductive electrodes, Angew. Chem. Int. Ed. 125 (21) (2013) 5645–5648.
[42] H. Li, Y.V. Aulin, L. Frazer, E. Borguet, R. Kakodkar, J. Feser, et al., Structure evolution and thermoelectric properties of carbonized polydopamine thin films, ACS Appl. Mater. Interfaces 9 (8) (2017) 6655–6660.
[43] R. Senga, T. Pichler, Y. Yomogida, T. Tanaka, H. Kataura, K. Suenaga, Direct proof of a defect-modulated gap transition in semiconducting nanotubes, Nano Lett. 18 (6) (2018) 3920–3925.
[44] C. Jolowsky, R. Sweat, J.G. Park, A. Hao, R. Liang, Microstructure evolution and self-assembling of CNT networks during mechanical stretching and mechanical properties of highly aligned CNT composites, Compos. Sci. Technol. 166 (2018) 125–130.
[45] S. Zhang, J.G. Park, N. Nguyen, C. Jolowsky, A. Hao, R. Liang, Ultra-high conductivity and metallic conduction mechanism of scale-up continuous carbon nanotube sheets by mechanical stretching and stable chemical doping, Carbon 125 (2017) 649–658.
[46] W. Han, H.-P. Zhang, J. Tavakoli, J. Campbell, Y. Tang, Polydopamine as sizing on carbon fiber surfaces for enhancement of epoxy laminated composites, Composites Part A 107 (2018) 626–632.
[47] I.H. Kim, T. Yun, J.E. Kim, H. Yu, S.P. Sasikala, K.E. Lee, et al., Mussel-Inspired defect engineering of graphene liquid crystalline fibers for synergistic enhancement of mechanical strength and electrical conductivity, Adv. Mater. 30 (40) (2018) 1803267.
[48] http://www.nanocomptech.com/. (Accessed November 10, 2018).
[49] http://carbonsolution.com/. (Accessed November 10, 2018).
[50] T.Q. Tran, Z. Fan, P. Liu, S.M. Myint, H.M. Duong, Super-strong and highly conductive carbon nanotube ribbons from post-treatment methods, Carbon 99 (2016) 407–415.
[51] Y. Shang, Y. Wang, S. Li, C. Hua, M. Zou, A. Cao, High-strength carbon nanotube fibers by twist-induced self-strengthening, Carbon 119 (2017) 47–55.
[52] S.Y. Cho, Y.S. Yun, D. Jang, J.W. Jeon, B.H. Kim, S. Lee, et al., Ultra strong pyroprotein fibres with long-range ordering, Nat. Commun. 8 (1) (2017) 74.
[53] Y. Jia, K. Li, L. Xue, J. Ren, S. Zhang, X. Zhang, Microstructure and mechanical properties of carbon fiber reinforced multilayered (PyC−SiC)n matrix composites, Mater. Des. 86 (2015) 55–60.
[54] Y. Jia, K. Li, L. Xue, J. Ren, S. Zhang, H. Li, Mechanical and electromagnetic shielding performance of carbon fiber reinforced multilayered (PyC-SiC)n matrix composites, Carbon 111 (2017) 299–308.
[55] S. Wu, M. Yi, Y. Ge, L. Ran, K. Peng, Effect of carbon fiber reinforcement on the tribological performance and behavior of aircraft carbon brake discs, Carbon 117 (2017) 279–292.
[56] Y. Wen, M. Wu, M. Zhang, C. Li, G. Shi, Topological design of ultrastrong and highly conductive graphene films, Adv. Mater. 29 (41) (2017) 1702831.
[57] http://www.ngfworld.com/en/en_fiber/en_high_thermal_conductivity.html. (Accessed November 10, 2018).
[58] S. Jiang, P.-X. Hou, M.-L. Chen, B.-W. Wang, D.-M. Sun, D.-M. Tang, et al., Ultrahigh-performance transparent conductive films of carbon-welded isolated single-wall carbon nanotubes, Science Advances 4 (5) (2018) 9264.
[59] http://www.matweb.com/. (Accessed November 10, 2018).
[60] Q.-M. Gong, Z. Li, Y. Wang, B. Wu, Z. Zhang, J. Liang, The effect of high-temperature annealing on the structure and electrical properties of well-aligned carbon nanotubes, Mater. Res. Bull. 42 (3) (2007) 474–481.
[61] L. Zhang, G. Zhang, C. Liu, S. Fan, High-density carbon nanotube buckypapers with superior transport and mechanical properties, Nano Lett. 12 (9) (2012) 4848–4852.
[62] W. Xu, Y. Chen, H. Zhan, J.N. Wang, High-strength carbon nanotube film from improving alignment and densification, Nano Lett. 16 (2) (2016) 946–952.
[63] G. Zhou, N.-R. Kim, S.-E. Chun, W. Lee, M.-K. Um, T.-W. Chou, et al., Highly porous and easy shapeable poly-dopamine derived graphene-coated single walled carbon nanotube aerogels for stretchable wire-type supercapacitors, Carbon 130 (2018) 137–144.